

SANDIA REPORT

SAND2018-13454

Printed November 2018



Sandia
National
Laboratories

Additively Manufactured Shock Absorbing Engineered Materials

Nicholas Leathe¹, Carolyn Seepersad², David Debeau², Audrey Morris-Eckart¹

1. Sandia National Laboratories, Albuquerque NM
2. University of Texas at Austin, Austin TX

Prepared by
Sandia National Laboratories
Albuquerque, New Mexico 87185
and Livermore, California 94550

Issued by Sandia National Laboratories, operated for the United States Department of Energy by National Technology & Engineering Solutions of Sandia, LLC.

NOTICE: This report was prepared as an account of work sponsored by an agency of the United States Government. Neither the United States Government, nor any agency thereof, nor any of their employees, nor any of their contractors, subcontractors, or their employees, make any warranty, express or implied, or assume any legal liability or responsibility for the accuracy, completeness, or usefulness of any information, apparatus, product, or process disclosed, or represent that its use would not infringe privately owned rights. Reference herein to any specific commercial product, process, or service by trade name, trademark, manufacturer, or otherwise, does not necessarily constitute or imply its endorsement, recommendation, or favoring by the United States Government, any agency thereof, or any of their contractors or subcontractors. The views and opinions expressed herein do not necessarily state or reflect those of the United States Government, any agency thereof, or any of their contractors.

Printed in the United States of America. This report has been reproduced directly from the best available copy.

Available to DOE and DOE contractors from

U.S. Department of Energy
Office of Scientific and Technical Information
P.O. Box 62
Oak Ridge, TN 37831

Telephone: (865) 576-8401
Facsimile: (865) 576-5728
E-Mail: reports@osti.gov
Online ordering: <http://www.osti.gov/scitech>

Available to the public from

U.S. Department of Commerce
National Technical Information Service
5301 Shawnee Rd
Alexandria, VA 22312

Telephone: (800) 553-6847
Facsimile: (703) 605-6900
E-Mail: orders@ntis.gov
Online order: <https://classic.ntis.gov/help/order-methods/>



ABSTRACT

This study investigates the static and dynamic mechanical performance of conformal negative stiffness honeycomb structures. Negative stiffness honeycombs are capable of elastically absorbing a static or dynamic mechanical load at a predefined force threshold and returning to their initial configuration after the load is released. Most negative stiffness honeycombs rely on mechanical loading that is orthogonal to the base of the structure. In this study, a more three-dimensional design is presented that allows the honeycomb to conform to complex surfaces and protect against impacts from multiple directions. The conformal designs are additively manufactured in nylon and stainless steel and subjected to quasi-static mechanical loading and dynamic mechanical impact tests that demonstrate their impact protection capabilities.

ACKNOWLEDGEMENTS

The authors would like to acknowledge Tommy Woodall, and Allen Roach of their support and guidance in this project. We would also like to thank Amanda Dodd and the rest of the Academic Alliance LDRD program for their role in getting this project funded.

CONTENTS

1. Introduction	7
2. Negative Stiffness Honeycombs	7
3. Metallic 2.5D Honeycomb.....	9
3.1. Quasi-Static Testing.....	9
3.2. Dynamic Evaluation.....	10
4. Conformal Elements	12
4.1. Metallic Conformal Element Fabrication	14
4.2. Metallic Conformal Element Evaluation	16
5. Conclusions	20

LIST OF FIGURES

Figure 1. Negative Stiffness Honeycomb.....	8
Figure 2. Experimental Quasi-Static Compression of a Negative Stiffness Honeycomb	8
Figure 3. Aluminum 2.5D Honeycomb.....	9
Figure 4: Computational Modeling vs. Quasi-Static Testing	9
Figure 5: Drop Test Rig at University of Texas at Austin.....	10
Figure 6: High Speed Impact Results. Experimental Data Compared to Simulation.....	10
Figure 7: Compressed Honeycomb	11
Figure 8: Uncompressed vs Compressed Honeycomb Dynamic Response	11
Figure 9. Conformal negative stiffness element (a) formed by revolving a unit cell cross section (b) about its central axis (c) and then removing four corners (d).	12
Figure 10: Conformal Elements Arranged in a Tiled Pattern.....	13
Figure 11: Dimensions for Nylon 11 Conformal Design.....	13
Figure 12: Dimensions for 17-4PH Stainless Steel Conformal Design.....	14
Figure 13: Metallic Test Element	14
Figure 14: Metallic Test Element – Build Orientation.....	15
Figure 15: Metallic Test Element – Selective Laser Sintered Fabricated	15
Figure 16: Metallic Test Element – Visibly Deformed from Heat Treatment.....	16
Figure 17: Quasi-Static Evaluation. Specimens 1, 2, and 3	16
Figure 18: Quasi-Static Evaluation. Specimen 4.....	17
Figure 19: SNL/NM Shock Lab Setup	17
Figure 20: Test Specimen #2, 11,700 g Impulse Input.....	18
Figure 21: Test Specimen #3, 7,900 g Impulse; Three Events.....	18
Figure 22: ABAQUS Model with Results	19
Figure 23: ABAQUS Model vs Specimen #2 Response	19
Figure 24: Load Shunting in 10,000 g Test.....	20

This page left blank

1. INTRODUCTION

An increase of computational modeling capability and tools has led to a deeper understanding of mechanical environments for our fielded systems. This deeper understanding, coupled with new environments for future system requirements, drives a need for shock mitigating materials and structures. These structures offer an opportunity to improve safety, reliability and security in countless products. Additive manufacturing offers significant advantages in the development of shock absorbing materials and structures as it increases product development agility, design freedom, and can be rapidly manufactured.

The idea of shock absorption could envelope an entire product, or protect only shock critical components. In each of these scenarios, minimizing the consumed volume is paramount. In practice, shock absorbing structures typically take the form of honeycomb material and are single use. That is, the structures dissipate energy through the plastic deformation of material and are unable to restore themselves to an original shape. The work accomplished in this project uses fully recoverable structures that are able to survive and respond to multiple shocks while maintaining a nominal response.

This project was done in partnership with Dr. Carolyn Seepersad at the University of Texas at Austin. She had previously demonstrated a plastic additively manufactured shock absorbing honeycomb material. This material was shown to reduce the peak response force of a dropped object by 1/20th with fully recoverable, elastic absorption mechanisms. The purpose of this project was to transform this idea into a usable product for Sandia National Laboratories. To do this, Sandia required the material change from plastic to metal to survive high temperatures; the design be modified to account for off-axis shock loading; and to dramatically increase the threshold to up to 15,000 g shocks.

2. NEGATIVE STIFFNESS HONEYCOMBS

An energy absorbing material or structure that responds elastically is ideal for Sandia products as it can recover from an initial impulse and continue to provide isolation through a series of subsequent impulses. Conventional honeycomb or octet-truss lattices provide lightweight stiffness and strength, however they use the plastic deformation of the material to absorb energy to provide isolation. To prevent the materials functionality from declining, these materials would be required to be replaced after use.

At the University of Texas at Austin, Dr. Carolyn Seepersad developed a plastic honeycomb-like material which was able to elastically respond to shock impulses while dissipating energy. The general shape for this can be noted in figure 1. This structure uses buckling to provide a force limit on the structure and enable a longer duration response of the structure to limit rate of input energy (acceleration) into the system.

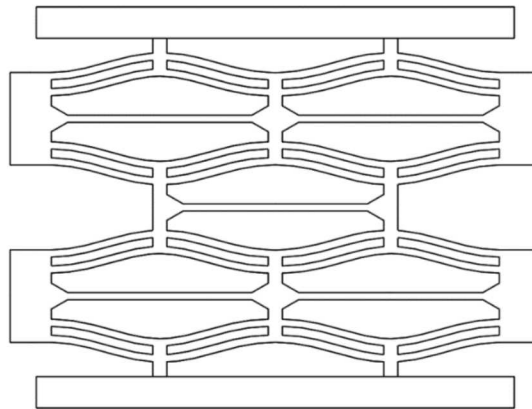


Figure 1. Negative Stiffness Honeycomb

Previous to the start of this project, Dr. Seepersad's work had evaluated a Nylon 11 selective laser sintered structure. It was about 5 inches long, 1.5 inches deep, and 4 inches tall. It was comprised of two rows and two columns of buckling elements, identical to figure 1. Figure 2, highlights the appeal of this structure. Here, through a quasi-static compression, the honeycomb limits the maximum force applied, despite the continued compression. The area between the curves is the energy dissipated by material hysteresis.

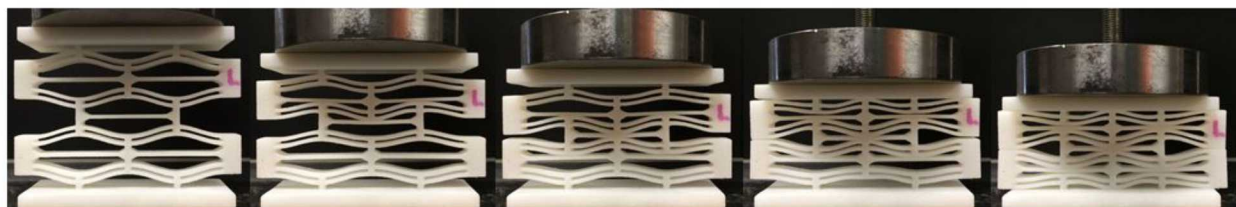
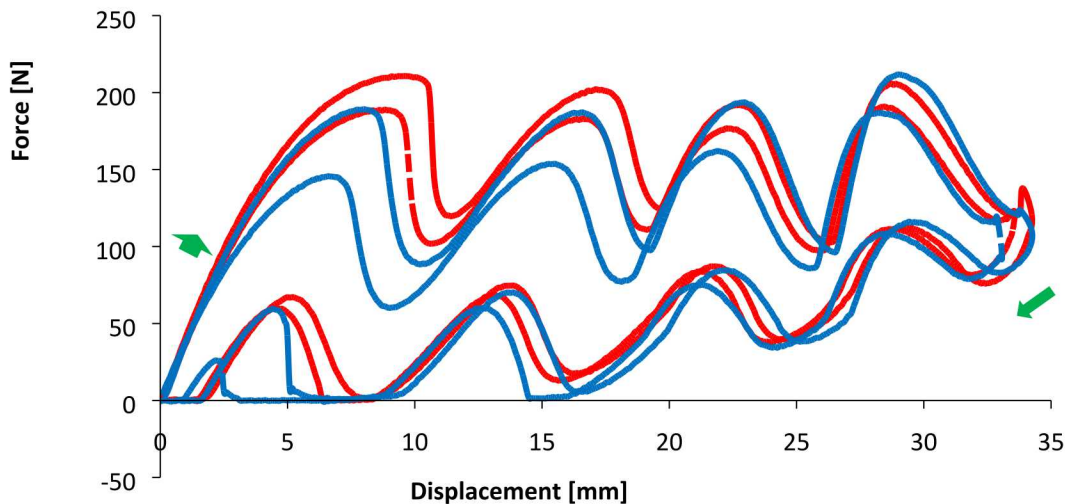


Figure 2. Experimental Quasi-Static Compression of a Negative Stiffness Honeycomb

3. METALLIC 2.5D HONEYCOMB

The first step for this project was to develop a metallic 2.5D honeycomb. This structure was to mimic the Nylon 11 design, but be tailored for the material properties of Aluminum 7075. The fabricated design was produced via water jet to reduce cost. This design was used to calibrate dynamic computational models. The overall design was about 6.5 inches long, 3.9 inches tall, and 0.5 inches thick. The individual beams were 78 mm long, 1 mm thick, and had an apex height of 2.2 mm.

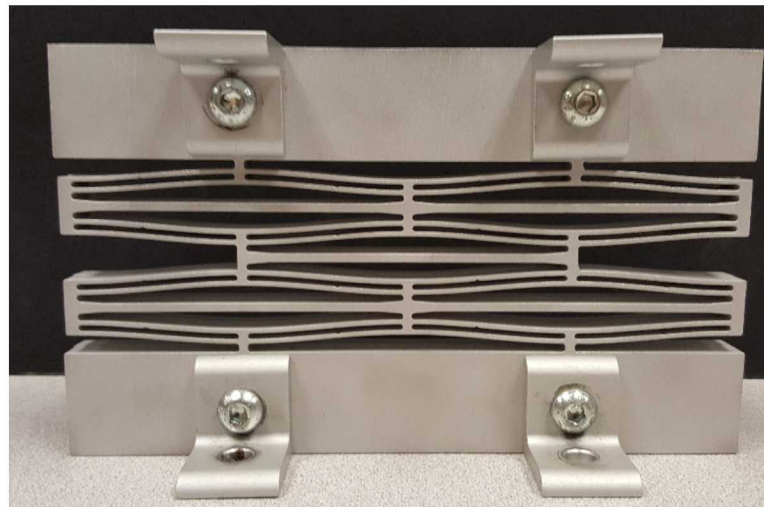


Figure 3. Aluminum 2.5D Honeycomb

3.1. Quasi-Static Testing

The metallic honeycomb was first evaluated using quasi-static displacement. These results were not as dramatic as the Nylon 11 material because aluminum does not have the inherent material hysteresis that Nylon 11 has, and thus the energy dissipation is much less noticeable.

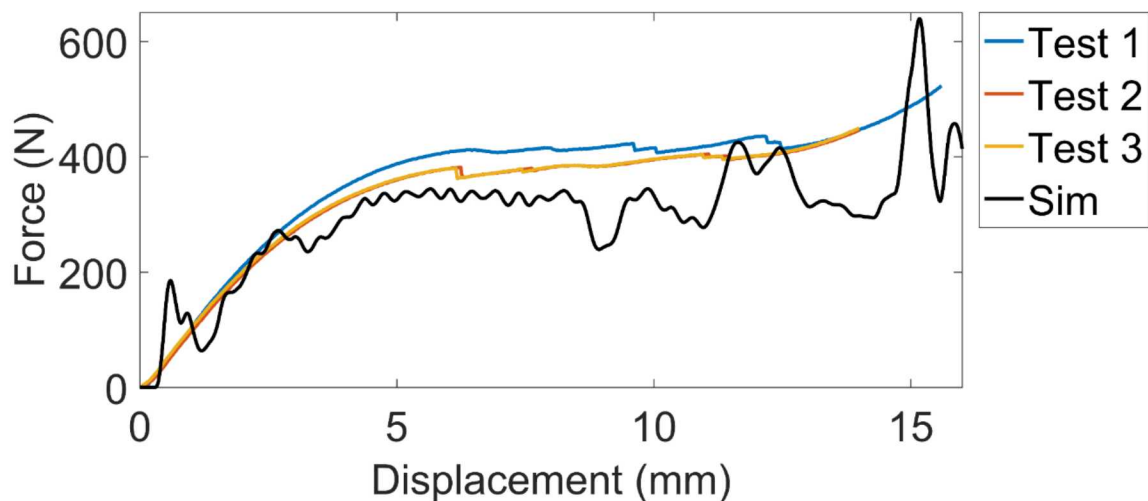


Figure 4: Computational Modeling vs. Quasi-Static Testing

3.2. Dynamic Evaluation

The dynamic evaluation of the aluminum honeycomb utilized a 5kg mass dropping from a height. The velocity immediately before impact was recorded using two graphite rods, spaced 6mm apart. These rods completed a 1V circuit and thus could be used to calculate the speed of the weight. The test setup is recorded in figure 5.

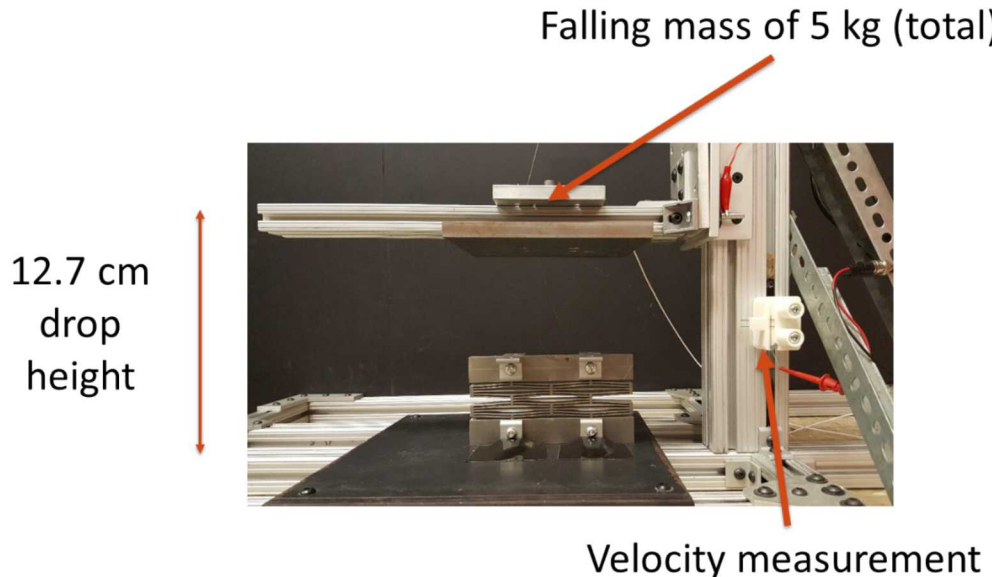


Figure 5: Drop Test Rig at University of Texas at Austin

The structure was tested under a series of evaluations. The data shown in figure 6 was recorded and modeled using a drop height of 17.8cm to achieve an impact velocity of 1.2 m/s. These parameters were then used to generate an ABAQUS simulation for predicting the results. As seen in figure 6, the model and the test align very well.

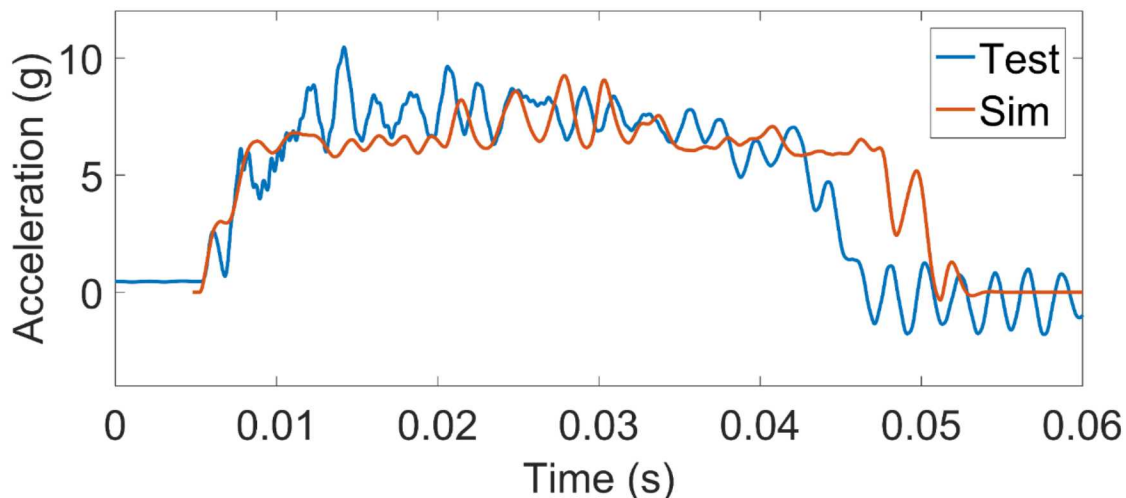


Figure 6: High Speed Impact Results. Experimental Data Compared to Simulation

The metallic honeycomb was compressed to a solid state for a comparison on the impact response without the negative stiffness structures. The experiment was repeated using the already compressed honeycomb to evaluate this difference. The uncompressed honeycomb had a response maximum of about 10gs while the compressed honeycomb had an impact response of about 67gs.



Figure 7: Compressed Honeycomb

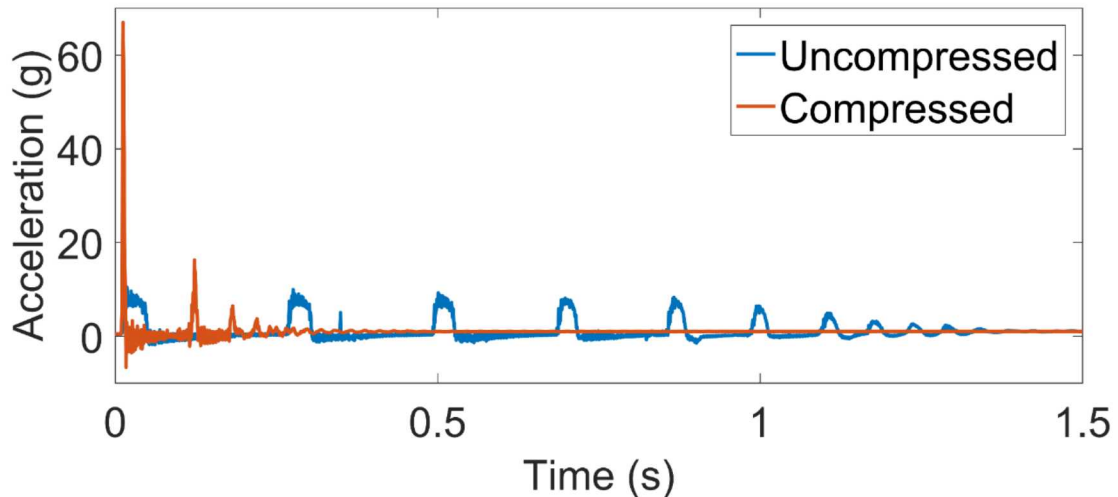


Figure 8: Uncompressed vs Compressed Honeycomb Dynamic Response

The testing and evaluation of the 2.5D metallic honeycomb demonstrated the dynamic models can accurately predict performance with metallic properties, high speed impacts, and much higher accelerations.

4. CONFORMAL ELEMENTS

The need for an element to mitigate off-axis shocks drove the design to a conformal negative stiffness element. The geometry for the conformal element leverages the profile of a 2.5D element and revolves the profile 360° around the central axis. Four corners are then removed from the element. This removal facilitates powder removal and enables the uniform tiling of elements conformally across a surface.

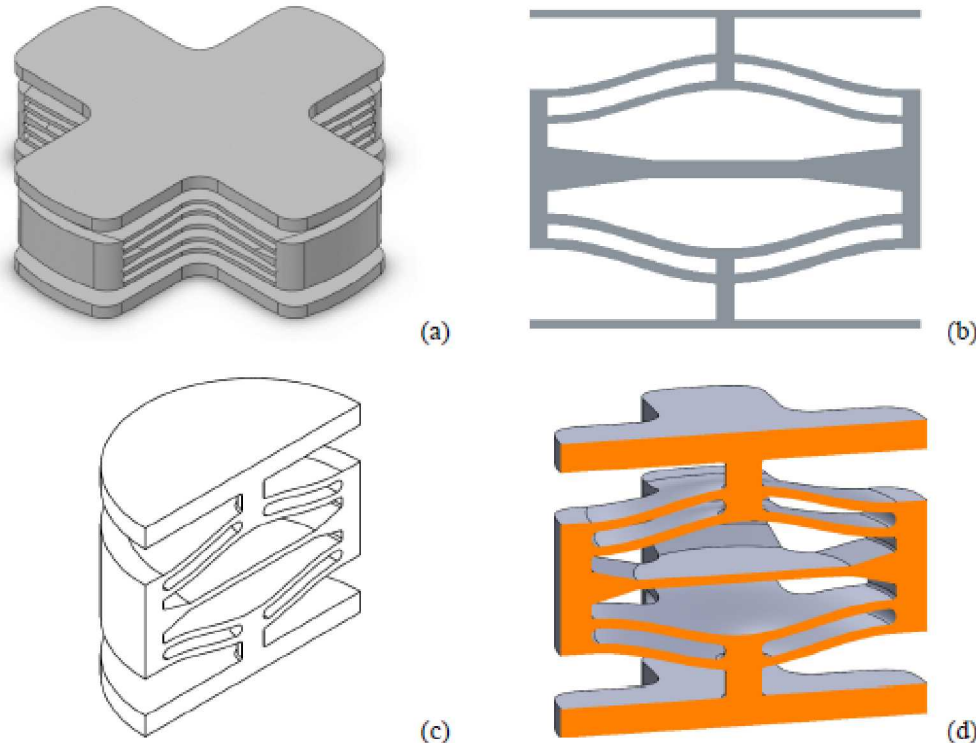


Figure 9. Conformal negative stiffness element (a) formed by revolving a unit cell cross section (b) about its central axis (c) and then removing four corners (d).

As previously noted, this design can be utilized to conformally coat a surface, regardless of curvature. The *plus* shape of the unit cell enables the designs to interlock as well, which can facilitate load sharing across multiple unit cells in different rows or columns.

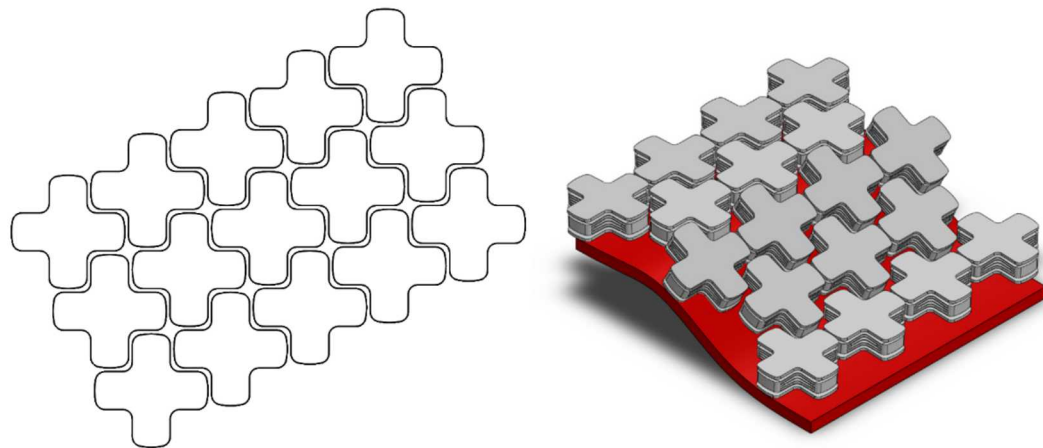
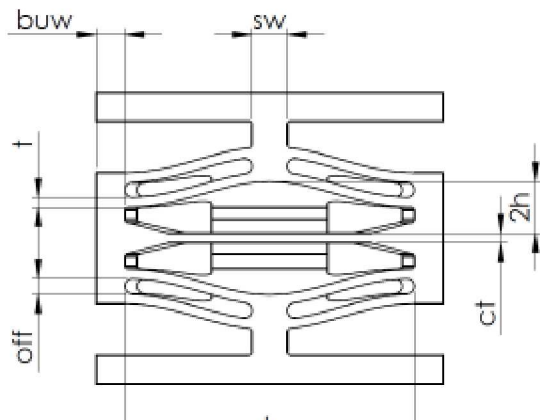


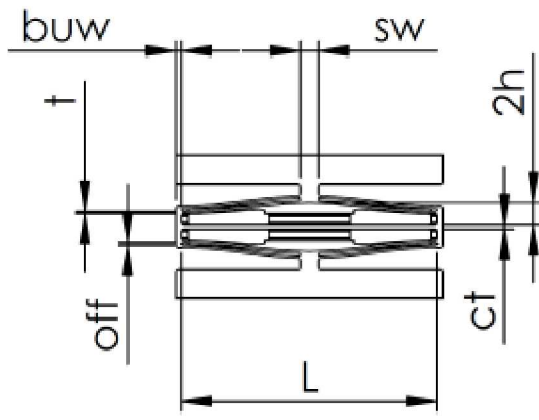
Figure 10: Conformal Elements Arranged in a Tiled Pattern

Conformal elements were fabricated with nylon 11 and 17-4PH stainless steel. The nylon dimensions are documented in figure 11. The curve of the beams are selected to achieve the prescribed force threshold, prevent beam yielding, and impact the bistability of the unit cell. The nylon structures were heavily utilized to calibrate models and evaluate performance of the conformal design at lower impact thresholds. The dimensions for the 17-4PH structures are documented in figure 12. These structures were utilized for the extreme impacts and are the focus of the remainder of the project.



Critical Dimension	Value (mm)
Beam Thickness (t)	1.66
Center Thickness (ct)	1.66
Beam Length (L)	50.0
Bistability (Q)	2.71
Beam Height (h)	$4.50 = Q * t$
Beam Offset (off)	$2.08 = 1.25 * t$
Bumper Width (buw)	5.00
Stem Width (sw)	6.00

Figure 11: Dimensions for Nylon 11 Conformal Design



Critical Dimension	Value (mm)
Beam Thickness (t)	0.50
Center Thickness (ct)	1.00
Beam Length (L)	56.3
Beam Height (h)	2.41
Bistability (Q)	4.81
Beam Offset (off)	0.625
Bumper Width (buw)	5.00
Stem Width (sw)	4.00

Figure 12: Dimensions for 17-4PH Stainless Steel Conformal Design

4.1. Metallic Conformal Element Fabrication

The metallic structures were fabricated on an EOS M270 with a layer thickness of 40 microns, using standard EOS 17-4PH build settings. From previous additive manufacturing projects, it was known that features as thin as 0.5 mm could be reliably sintered. This dimension was selected as the beam thickness to maximize the beam height without exceeding the allowable yield strain of the material. The test specimen also included mounting holes to simplify test fixturing, as shown in figure 13. A total of four specimens were manufactured. The specimens were fabricated on their side, as shown in figure 14, to minimize the amount of support material required to reliably print the geometry.

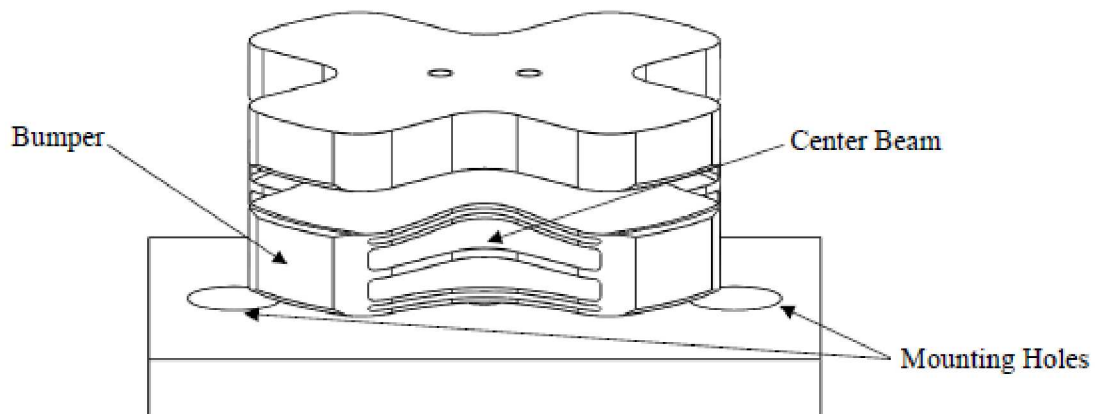


Figure 13: Metallic Test Element

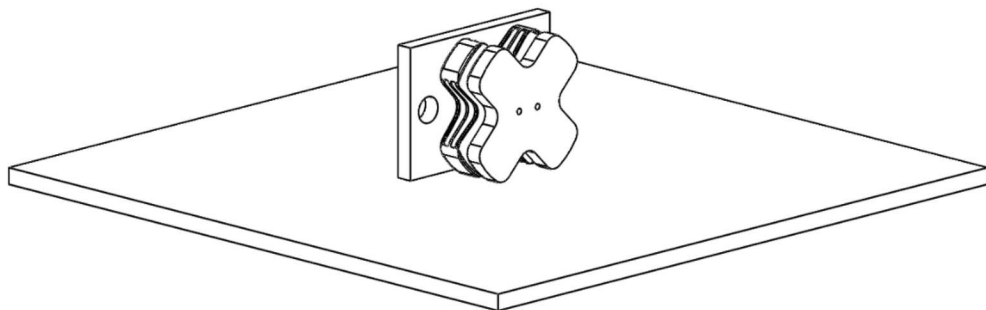


Figure 14: Metallic Test Element – Build Orientation

After the sintering process, the entire build plate was heated to a temperature of 1900 °F for an hour and then air cooled. This reduced the residual stress in the part and helped prevent warping after the parts were removed from the build plate. A sintered part is shown in figure 15. After removal from the build plate, additional holes for accelerometers were added, and the mounting holes were post machined.



Figure 15: Metallic Test Element – Selective Laser Sintered Fabricated

After post-machining the parts, the specimens were subjected to Hot Isostatic Pressing (HIP) to minimize part porosity. The HIP process subjected the parts to 2125 °F at 14.75 ksi for four hours. The specimens were then hardened using a standard H1150 heat treatment process. This required heating the parts to 1150 °F for an additional four hours and then air cooling. During the HIP and heat treatment processes, the parts were oriented as shown in figure 15. This allowed the parts to deform and sag under their own weight, modifying the intended geometry of the unit cell. Three of the four fabricated specimens were deformed, while one unit was held back and treated differently. An image of the deformed geometry can be seen in figure 16.

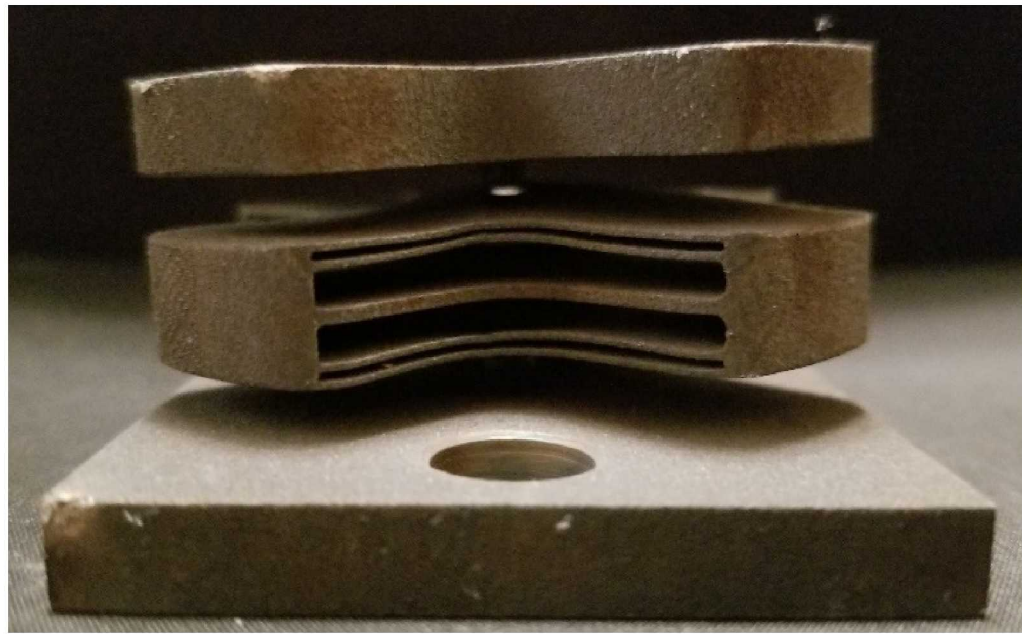


Figure 16: Metallic Test Element – Visibly Deformed from Heat Treatment

4.2. Metallic Conformal Element Evaluation

The metallic elements were initially quasi-static tested to evaluate their initial behavior. In this dataset, specimens 1, 2, and 3 were damaged in the HIP and heat treatment processing; while unit 4 was post-processed as designed. In the quasi-static evaluation, each of the original three units experienced some behavioral run-in, but then converged. Figure 17 shows the quasi-static tests for specimens 1, 2, and 3. Figure 18 shows the first three tests for specimen 4.

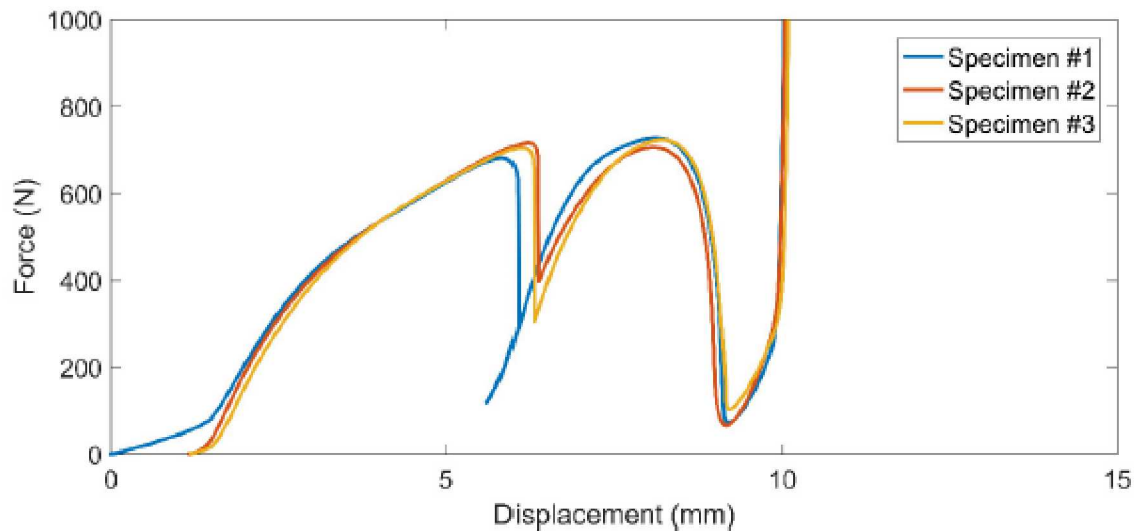


Figure 17: Quasi-Static Evaluation. Specimens 1, 2, and 3

The run-in behavior demonstrated in figure 18 is likely due to a small amount of plastic deformation and work hardening of the material. Despite this phenomena, tests 2 and 3 are very repeatable. Comparing the undamaged unit to the damaged units, the force thresholds remain about the same, showing design robustness to manufacturing defects.

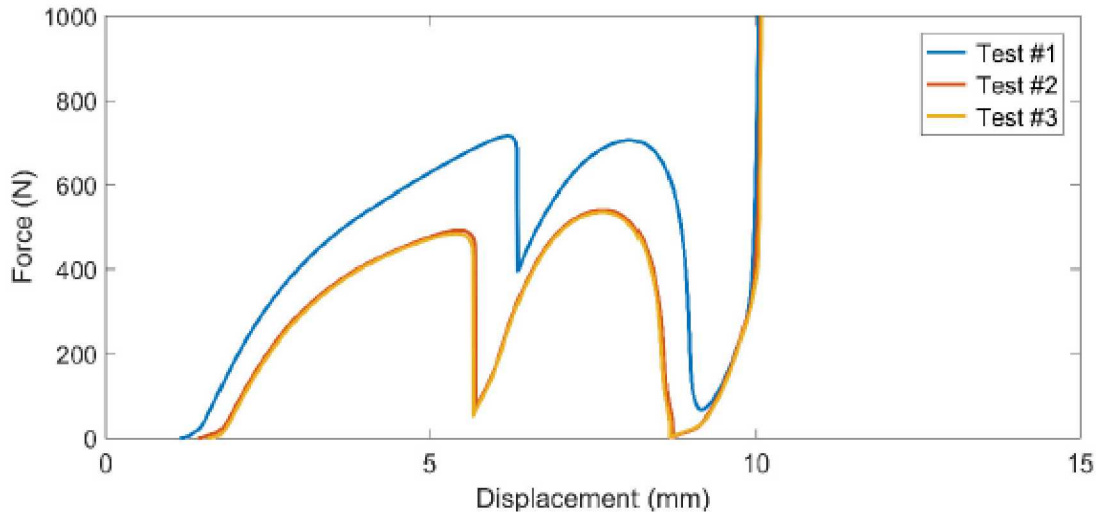


Figure 18: Quasi-Static Evaluation. Specimen 4

The metallic elements were tested at the Shock Lab at Sandia National Laboratories in Albuquerque, NM. This test facility provided an opportunity to test the structures at much higher shock amplitudes than at the University of Texas at Austin, and offered additional capability in terms of high speed data recording and high speed cameras. Figure 19 shows the test setup used to evaluate these specimens.

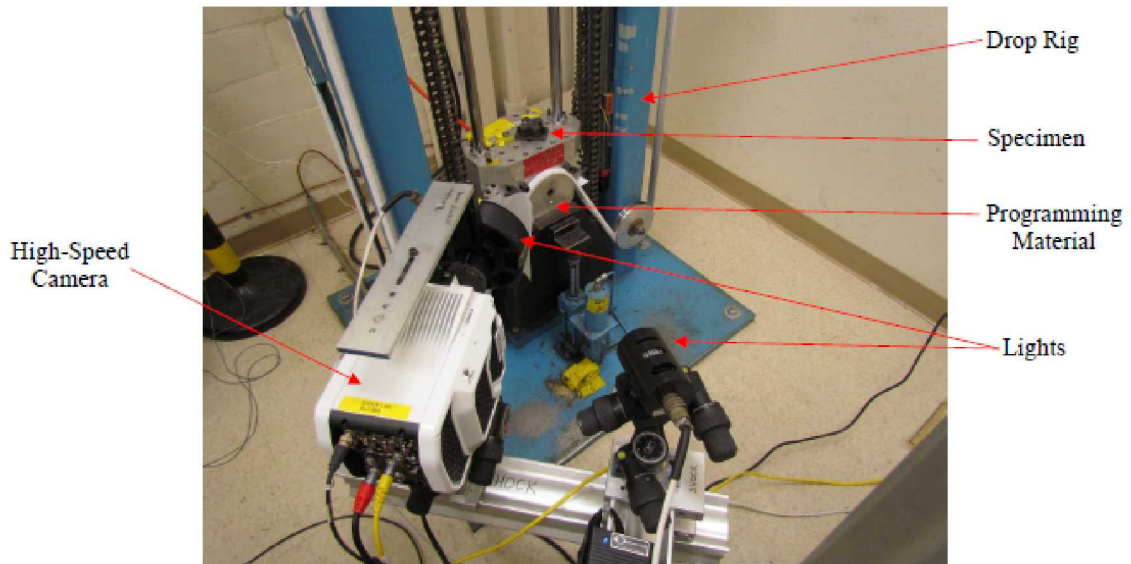


Figure 19: SNL/NM Shock Lab Setup

For the drop tests, accelerometers were placed on the drop carriage and the top of the specimen. The carriage accelerometer is assumed to be the resulting shock for an object without negative stiffness protection, while the top of the specimen would be the protected object.

Across all of the tests, a dramatic improvement to the impact response was demonstrated, even with the damaged units. In figure 20, specimen 2's response to an 11,700 g impulse is shown. The top of the specimen measured a peak acceleration of 758.3 gs versus the peak carriage acceleration of 11,700 gs. It should be noted that the peak of the impact is dramatically reduced, however the duration of the event is much longer for the top of the specimen (red curve).

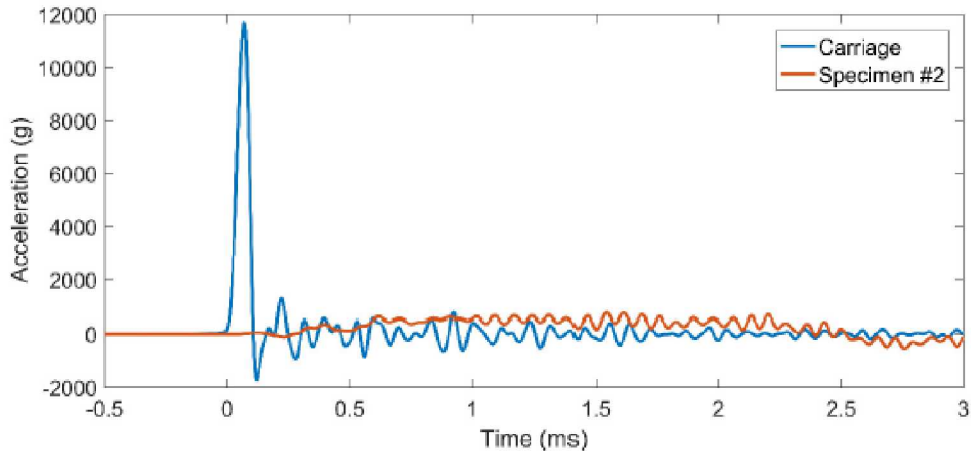


Figure 20: Test Specimen #2, 11,700 g Impulse Input

In terms of repeatability for the individual units, test specimen 3 was tested at three levels with approximately the same input impulse. In these tests, the specimen has an almost identical reaction to the input, providing evidence that the specimen's reaction is very repeatable. It should be noted that these tests were done after the quasi-static tests, so there is no additional run-in behavior for the specimens.

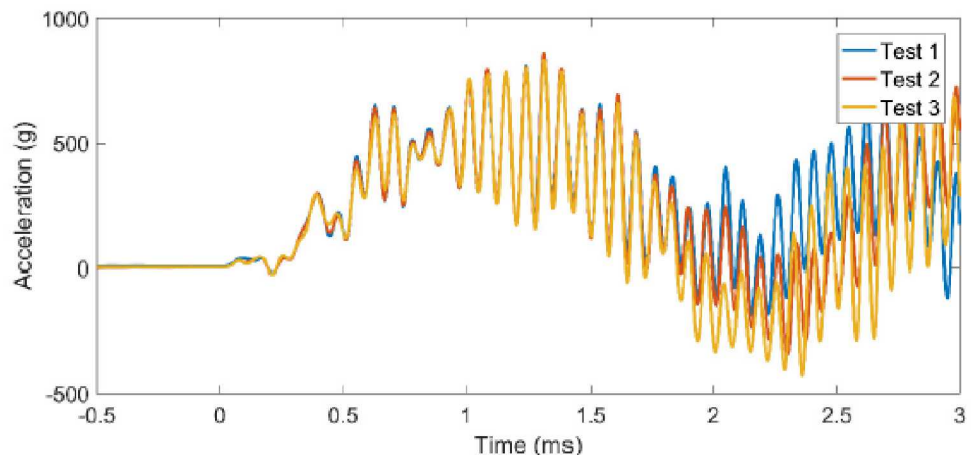


Figure 21: Test Specimen #3, 7,900 g Impulse; Three Events

A significant amount of effort went into developing an ABAQUS model for the metallic structures. In the computational models, the acceleration is integrated over a simulated haversine impulse. This velocity change is applied to a set of constrained nodes at the bottom of the specimen. For the case of a 15,000 g, 0.1 ms impulse, the initial velocity of the cell is prescribed to -7.355 m/s and as the simulation begins, the bottom nodes decelerate using the integrated shock impulse. Figure 22 shows the meshed finite element model with a graph of the velocity for the bottom, constrained node, and the top node.

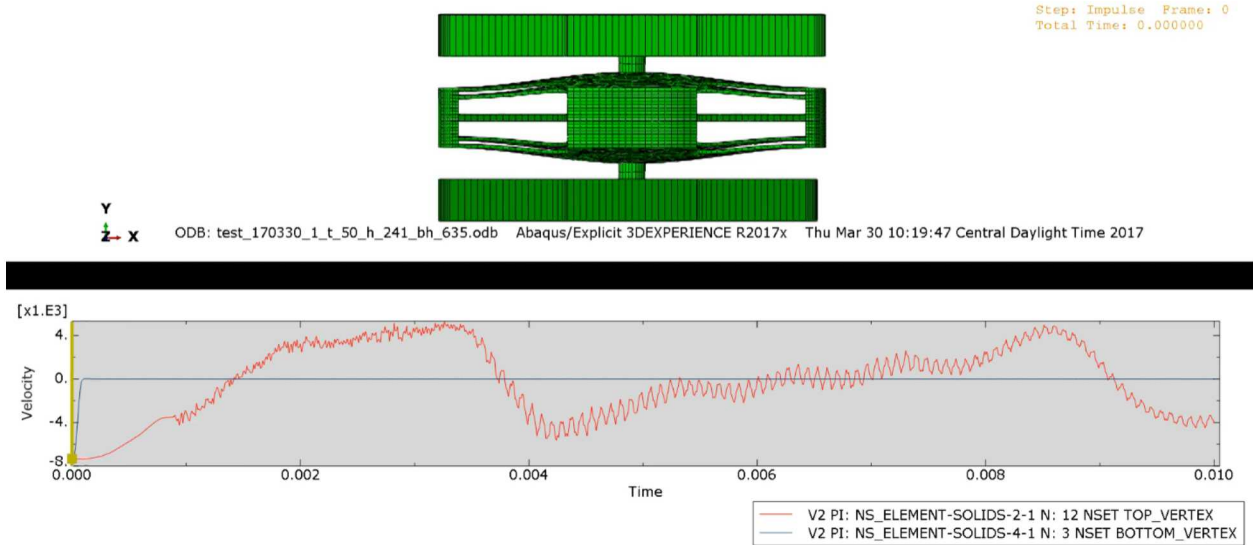


Figure 22: ABAQUS Model with Results

Comparing the results of the finite element model to the testing, the differences between the two are quite small. As previously noted, the physical test saw a loading of 758.3 g and the model predicted a response of 784.8 g. These results are shown in figure 23.

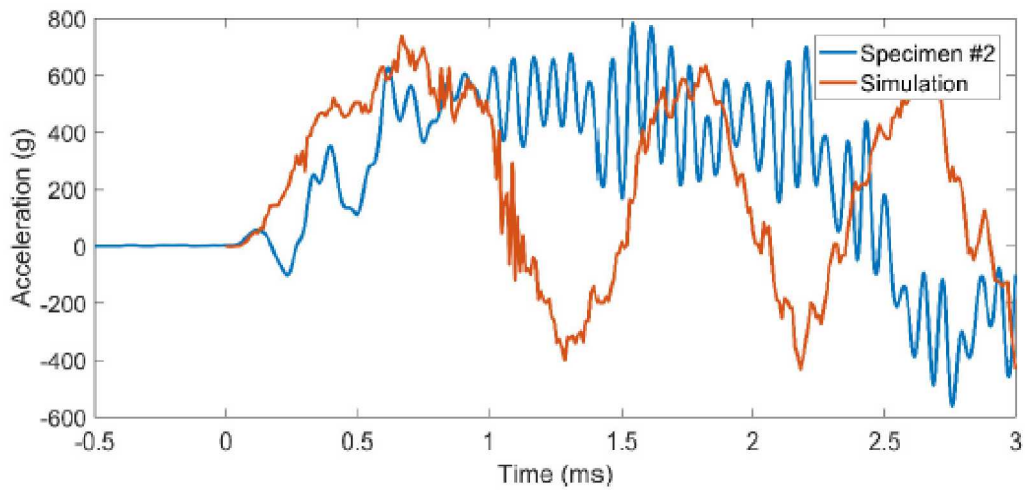


Figure 23: ABAQUS Model vs Specimen #2 Response

It should also be noted that because of the damage induced to specimens 1, 2, and 3, higher testing could not be accomplished. Originally the parts were designed to a maximum level of 15,000g, but at the 10,000g threshold the honeycomb collapsed at an angle, causing a large spike in acceleration and shunting the load into the side of the specimen. At higher testing levels, this behavior was expected to continue and thus was not tested. This phenomena is shown in figure 24.

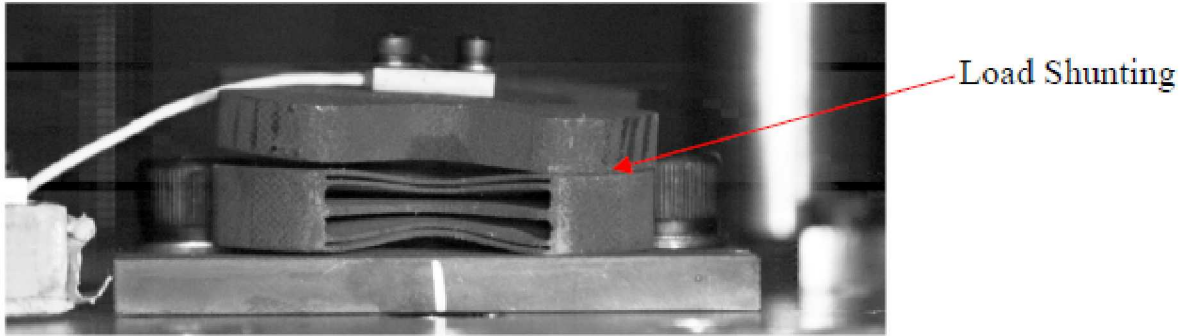


Figure 24: Load Shunting in 10,000 g Test

5. CONCLUSIONS

Over the course of this project, the 2.5D nylon 11 negative stiffness design has transformed into a 3-dimensional object that could conformally coat curved surfaces. It has been manufactured out of high strength metal and evaluated to demonstrate functionality. This research couples with ABAQUS dynamic modeling to model the performance of such elements to enable the capability to predict the behavior prior to unit cell fabrication. The end result is the capability development to enable engineers to utilize these structures to mitigate severe environments by providing an insulative layer of elements, and improve the overall safety, reliability, and security of their design.

DISTRIBUTION

Email—Internal

Name	Org.	Sandia Email Address
David Minster	1174	dgminst@sandia.gov
Shawn Dirk	1830	smdirk@sandia.gov
D. Chavez, LDRD Office	1911	dchavez@sandia.gov
Tommy Woodall	2180	twooda@sandia.gov
Allen Roach	2441	raroach@sandia.gov
Jared McLaughlin	2610	jtmclau@sandia.gov
Audrey Morris-Eckart	2616	amorri@sandia.gov
Justine Johannes	6600	jejohan@sandia.gov
Bonnie Antoun	8343	brantou@sandia.gov
Amanda Dodd	8366	ajbarra@sandia.gov
John P. Sullivan	8713	jpsulli@sandia.gov
Technical Library	9536	libref@sandia.gov



**Sandia
National
Laboratories**

Sandia National Laboratories is a multimission laboratory managed and operated by National Technology & Engineering Solutions of Sandia LLC, a wholly owned subsidiary of Honeywell International Inc. for the U.S. Department of Energy's National Nuclear Security Administration under contract DE-NA0003525.